Direct Antenna Modulation (DAM) with Switched Patch Antenna– Performance Analysis

Hengzhen Crystal Jing [1], Xiaojing Jessie Xu [2], and Yuanxun Ethan Wang [2]

[1] QuinStar Technology Inc.
Torrance, CA 90505, U.S.A.

[2] Department of Electrical Engineering
University of California at Los Angeles, Los Angeles, CA 90095, U.S.A.
ywang@ee.ucla.edu

Abstract ─ Resonant antennas, such as patch antennas, can be directly modulated with high speed switch devices that were integrated onto the radiation aperture, as the radiation can be turned on or shut off in real-time. Such an antenna is found to be able to radiate pulses with rich spectrum components far beyond the antenna's originally defined bandwidth. In this paper, the efficiency bandwidth product of such an antenna is examined to determine whether it can potentially surpass the usual limit defined by the antenna quality factor. For this purpose, a thorough study on the time-varying behavior of a directly modulated microstrip patch antenna is carried out. The theoretical performance of such an antenna in its radiation power and efficiency is discussed. The time-domain analysis starts with the transmission line model of the patch antenna and the equivalent circuit models. A full-wave Finite Difference Time Domain (FDTD) code that incorporates time-varying switching devices in its mesh is then used to simulate the dynamics of the antenna. The study has demonstrated the capability of improving the radiation efficiency and bandwidth performance over the conventional 1/Q limit, with the so-called Direct Antenna Modulation (DAM) technique.

Index Terms ─ Direct antenna modulation, impulse radio, switched resonator, time-varying systems and ultra-wideband antennas.

I. INTRODUCTION

Ultra-Wideband (UWB) antennas are traditionally designed in the frequency domain by enlarging their impedance matching bandwidth. However, transmitting broadband pulse signals not only requires the antenna to radiate energy across a broad spectrum, but also a linear phase response and a constant radiation pattern over the frequency band so that the pulse shape is not distorted [1-3]. It is difficult for existing broadband antennas to meet these requirements, especially when the antenna dimension is constrained. Recently, Direct Antenna Modulation (DAM) techniques have been proposed to radiate pulses from a narrow band antenna [4-10]. Instead of using the antenna as a passive component of the transmitter, the antenna is directly modulated through turning on and off the integrated switch devices. Different from those in reconfigurable antennas [11-15], the purpose of using switching devices on the antenna in DAM systems, is to create boundary conditions that are varying in real time. A number of experiments [6-8] have demonstrated that a DAM system with a switched microwave patch antenna can radiate rich spectrum components beyond the original antenna bandwidth limit. Similar techniques have been proposed and experimented [16-18] for high power impulse radiations through TEM horn antennas. With DAM techniques, it is possible to simplify the design of a broadband wireless transmitter by transmitting high speed pulses from antennas with low profiles and simple feeding structures or even electrically small antennas [19].

This paper is to study the theoretical potential of the DAM on whether or how it can overcome the conventional limit of efficiency bandwidth product in a high-Q antenna system [20]. In a

Submitted On: June 8, 2013
Accepted On: April 17, 2014

conventional antenna system, the antenna gain and efficiency drops as the radiation bandwidth is enlarged. In a DAM system, the loss of the switches certainly degrades the antenna efficiency to some extent depending on the available semiconductor technology. An even more fundamental loss mechanism in DAM is the energy loss due to the switching action itself, which may happen when a non-zero-voltage capacitor is short-circuited or a non-zero-current inductor is open-circuited. This type of phenomena can not be predicted by frequency domain analyses, but a complete study of the time-domain behavior of the antenna. In this paper, the transient behavior of a directly modulated microstrip patch antenna is obtained in the following three steps. First, the energy building up and release process in the antenna resonator is observed. Second, a bounce diagram analysis with the transmission-line equivalence of the antenna is performed. Lastly, 3-D full-wave simulations are carried out based on a Finite Difference Time Domain (FDTD) code that incorporates non-linear devices in its mesh. From those analyses, the power and efficiency performance is analytically derived and quantitatively evaluated. It is discovered that the energy conversion between the storage mode and radiation mode in time domain dominates the overall performance of the DAM system. To achieve high radiation efficiency, one needs to mount switch devices on one edge of the antenna and switch them at the zero-voltage moment, in order to avoid the energy loss due to the switching action itself. Another interesting phenomenon is that the instantaneous power of the short pulses radiated after switching can be greater than the available source power at the antenna input, which is related to the pulse compression phenomenon of switched resonators [21]. Similar phenomena have also been observed in [16-18].

II. PHYSICAL PRINCIPLE

A microstrip patch antenna integrated with switches is used as an example to test the performance of DAM. The physical structure of the antenna is illustrated in Fig. 1 (a). The length of the patch between two radiation edges is approximately half of a substrate wavelength at the desired radiation frequency. The antenna is excited by a single-tone RF source through a feeding probe, with the frequency coinciding with the antenna's resonant frequency to inject the carrier energy to the antenna, as shown in Fig. 1 (a). A number of switch devices, such as diodes or transistor switches connecting the top patch to the ground plane are mounted at one of the radiation edges, while the other edge is connected to the ground through a perfect conductor strip. The switches are driven by a modulation signal that controls the radiation through the biasing voltages. As it will be explained in the latter sections, short-circuiting the other radiation edge is to provide a complete period of continuous radiation. The two non-radiation edges can be considered to be terminated by Perfect Magnetic Conductor (PMC). Thus, the equivalent cavity model of this particular patch antenna is derived as Fig. 1 (b). When the switches are turned on, the structure behaves like a cavity that resonates at the carrier frequency and supports the TEM mode as its fundamental cavity mode. The radiation behavior of the antenna under switching in real-time is determined by both the antenna's transient behavior and the device's characteristics. A simplified analysis, however, is possible when the process of energy accumulation and release in resonant antennas is followed step-by-step. For example, the following steps are taken for each radiation/storage cycle:

1. Switches are turned on: the patch antenna works as a resonator that starts to accumulate the RF energy at the resonant frequency f_c in the antenna.
2. RF energy is being injected into the antenna resonator. No radiation is created at this stage, except the leakage from non-radiation edges. The antenna operates in a non-radiating resonant mode, which is characterized with a half-sinusoid distribution spatially in its vertically polarized electric field, with two zeros at the edges and the maximum in the center.
3. Energy dissipation in the antenna eventually reaches the same rate as the energy injection. Sources of energy dissipation include Ohmic and dielectric losses of the antenna, leakage from the non-radiation edges and conduction loss on switch devices.
4. Switches are turned off: the previous resonant boundary condition is changed. The electric field at the radiating slot appears immediately and starts to form magnetic currents radiating into the free space. As the

radiation is from the previously stored energy that is accumulated to a great amount, the instantaneous power radiated can be greater than the injected power through pulse compression [21].

5. Radiation continues for a certain period before the discontinuity in the electric field appears at the radiating aperture. The length of the patch determines this delay. For example, the current λ/2 design allows the continuous radiation of one RF cycle without seeing discontinuity in the radiation. The radiated spectrum of monopulse is an ultra-wideband spectrum centered at the injected carrier frequency.
6. When the switch is kept off for more than one RF cycle, the radiated wave will change its phase by 180 degrees for every RF cycle. The radiated spectrum will now be shifted to be clusters around the ($f_c/2$, $3f_c/2$…), instead of the original RF frequency, as it is supported by the λ/4 mode and the odd-integer higher order modes of the patch in the frequency domain.
7. Switches are turned on again after the radiation lasts for an integer number of cycles. The antenna returns to the storage mode at the original resonant frequency.

Therefore, with switches turned on and off in a certain pattern through the above steps, information can be coded into the radiation with modulation methods, such as pulse width or position modulations [22].

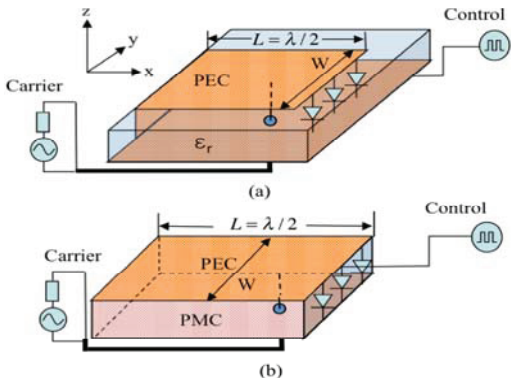

Fig. 1. (a) Physical structure of the patch antenna for pulse transmission and (b) equivalent cavity model of the patch antenna.

III. TRANSMISSION LINE ANALYSIS

The transmission line equivalence model [23] applies when only the dominant mode of the patch is considered and it characterizes the field underneath the patch as a TEM wave bouncing back and forth between the two radiation edges. The model includes the excitation, the short circuit on one of the edges, the switches on the other edge and the radiation impedance of the slot on that edge, as shown in Fig. 2. L is the length of the patch and L_1 is the length between the feeding to the switched edge. R_s is the source impedance in the excitation, R_{on}/R_{off} is the total on/off resistance of the switches and G_r and B_r are the radiation conductance and susceptance of the radiating slot, respectively. It is practical to assume $R_{off} >> R_r$. When the switches are on, the structure becomes a transmission-line resonator with both ends short-circuited. This allows a standing wave between two edges. Once the switches are turned off, the resonant condition changes.

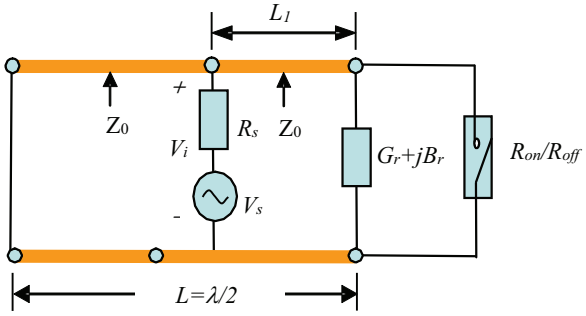

Fig. 2. Transmission line model of the switched mode microstrip antenna.

In order to observe how the field structure evolves in real time following the switching, the standing wave is separated into forward and backward propagating waves and the voltage is formulated in (1);

$$\Phi(t,z) = f^{+}(t,z) + f^{-}(t,z), \tag{1}$$

and

$$f^{+}(t,z) = A^{+}\cos(\omega t - kz), \tag{2a}$$

$$f^{-}(t,z) = A^{-}\cos(\omega t + kz), \tag{2b}$$

where $0 \le z \le L$, A^{+} and A^{-} are the amplitudes of the forward and backward propagating waves. During the switch-on period, the voltage at the two edges satisfies the boundary conditions:

$$\Phi(t, z=0)=0\,, \qquad \Phi(t, z=L)=0, \tag{3}$$

which gives:

$$A^{-}=-A^{+}. \tag{4}$$

This also implies that the forward and backward propagating waves are of equal amplitude and 180-degree phase difference so that they cancel with each other completely on two edges. The final voltage distribution underneath the patch is thus given by:

$$\Phi(t,z)=A^{+}[\cos(\omega t-kz)-\cos(\omega t+kz)]. \tag{5}$$

Once the switches are turned off at the moment t_0, the boundary condition at the radiation edge instantly becomes a high impedance value. This value is approximately given by the radiation impedance of the slot when the edge capacitance is neglected. The reflection coefficient at that edge changes from -1 to approximately 1 and the backward propagating wave is flipped in polarity starting from that moment, e.g., $A^{-}\approx A^{+}$. To reveal how the field structure changes in time-domain, bouncing diagrams for both forward and backward propagating waves are generated as the functions of both time and position in the following:

Case 1: $t_0 \le t < t_0 + T/2$;

$$f^{+}(t,z)=A^{+}\cos(\omega t-kz) \qquad 0\le z\le\frac{\lambda}{2}, \tag{6a}$$

$$f^{-}(t,z)=\begin{cases} -A^{+}\cos(\omega t+kz) & 0\le z<(\frac{\lambda}{2}-\frac{t-t_0}{T}\lambda) \\ A^{+}\cos(\omega t+kz) & (\frac{\lambda}{2}-\frac{t-t_0}{T}\lambda)\le z\le\frac{\lambda}{2} \end{cases}. \tag{6b}$$

Case 2: $t_0 + T/2 \le t < t_0 + T$;

$$f^{+}(t,z)=\begin{cases} -A^{+}\cos(\omega t-kz) & 0\le z<(\frac{t-t_0}{T}\lambda-\frac{\lambda}{2}) \\ A^{+}\cos(\omega t-kz) & (\frac{t-t_0}{T}\lambda-\frac{\lambda}{2})\le z\le\frac{\lambda}{2} \end{cases}, \tag{7a}$$

$$f^{-}(t,z)=A^{+}\cos(\omega t+kz) \qquad 0\le z\le\frac{\lambda}{2}. \tag{7b}$$

The bouncing diagram is simulated in MATLAB based on Eq. (6-7) and plotted in Fig. 3 by setting A^{+}=1. The voltages are combined to demonstrate the final voltage distribution underneath the patch at each snapshot. In each plot, the two dashed lines represent voltage distribution of the forward and the backward propagating waves at a time snapshot along the longitudinal direction, while the solid line indicates the combined voltage. The first plot shows a standing wave pattern as the result of the antenna resonance at the beginning of the time coordinate. Immediately after that, the switches are turned off and the instantaneous voltage distribution is plotted for every quarter of the carrier cycle, as displayed in Fig. 3 (b-f).

It is evident that the voltage at the radiation edge is no longer zero after the switches are turned off, but given by the constructive summation of the two waves. This indicates the emergence of the radiation associated with a non-zero magnetic current on that edge. The magnetic current behaves as a sinusoid function of time and lasts continuously for one RF cycle, as shown in Fig. 3 (b-f). There will be a 180 degree phase shift in the magnetic current after one RF cycle and if the switches remain off, as the voltage discontinuity in the backward wave resulting from switching action arrives at the radiation edge after it has traveled a round trip through the transmission line. Therefore, the switches should be turned on right before the discontinuity happens so that the magnetic current appears as a complete monocycle pulse on the radiating slot. The radiated field is directly related to the magnetic current and should also be a pulse. Therefore, if the edge capacitance is neglected, the radiation can rapidly start and stop without the typical delay caused by the high-Q bandpass behavior of the patch antenna.

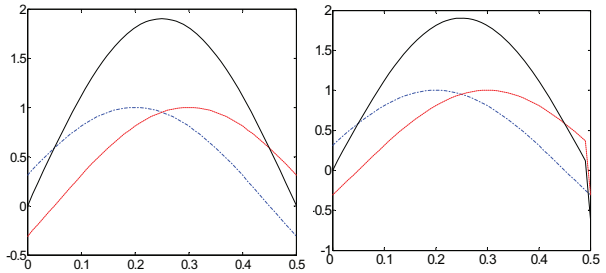

(a) $t=0^{-}T$ (switch on) (b) $t=0^{+}T$ (switch off)

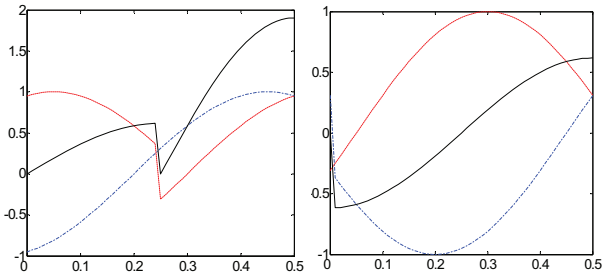

(c) $t=1/4T$ (d) $t=1/2T$

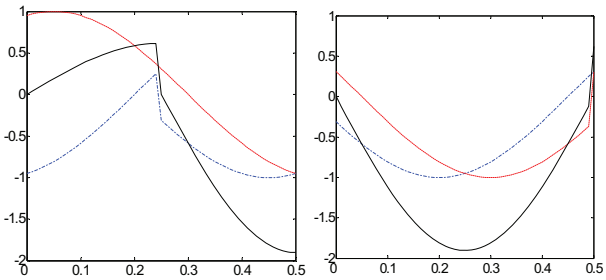

(e) *t=3/4T* (f) *t=1T*

Fig. 3. Time variation of the voltage distribution along the longitudinal direction underneath the patch during the switching process (forward –-, backward --- and total —).

IV. PULSE COMPRESSION AND RADIATION

According to the analysis in section II, the instantaneous power from the antenna in a DAM system radiated immediately after the switches are turned off, which is determined by the initial energy stored in the non-radiating mode. The amount of stored energy is related to the charging time and the Q-factor of the antenna resonator for the switch-on case. If lower on-resistance switches (higher Q-factors) and longer charge times are used, the instantaneously radiated power over a short duration can be greater than that of conventional patch antennas driven by a single-tone carrier. This is the so-called pulse compression phenomenon which exists in many switched resonant structures and has been well described in [20]. For the same amount of input power, one may define the pulse compression gain as the ratio between the instantaneously radiated power during the pulse-on period in the DAM scheme, versus the radiated power in a conventional antenna. The pulse compression gain generally increases when a longer charging time is used until the antenna resonator is fully charged, whereas the maximum pulse compression gain is reached. The maximum achievable pulse compression gain is related to the energy storage capacity of the antenna. For an antenna represented by the transmission line model in Fig. 2, the maximum pulse compression gain is derived to be [See Appendix I]:

$$G_{pulse,\max} = \frac{Z_0^2}{R_{on} R_r}. \tag{8}$$

The maximum pulse compression gain is higher than 1 when the following condition is satisfied:

$$R_{on} < \frac{Z_0^{\,2}}{R_r}, \tag{9}$$

which necessitates high-speed and low-resistance switches. The gain does not come from any active device, but from the energy compression into shorter time duration by the direct antenna modulation scheme. The pulse compression gain relationship denoted by (8) can be generalized in terms of the Q factors of the antenna resonator. The antenna operates alternatively between the storage phase and the radiation phase. In the storage phase, the switches are on and the field behaves in a half wavelength transmission line resonator mode, while in the radiation phase the switches are turned off and the field follows a quarter-wave transmission line resonator mode. By ignoring the edge susceptance, one can find that the Q factors of the transmission line resonators for the switch-on and off cases are given by:

$$\begin{cases} Q_{on} = \dfrac{\pi}{4}\dfrac{Z_0}{R_{on}} & \text{(switch on or pulse off)} \\ Q_{off} = \dfrac{\pi}{4}\dfrac{R_r}{Z_0} & \text{(switch off or pulse on)} \end{cases}. \tag{10}$$

In conjunction with (8), it leads to:

$$G_{pulse,\max} = \frac{Q_{on}}{Q_{off}}, \tag{11}$$

which is a general expression of the pulse compression gain independent of antenna structures. From (11), it is obvious that in order to achieve a high pulse compression gain, one needs to keep the highest possible Q in the storage mode and the lowest possible Q in the radiation mode. The former requires minimizing the dissipation of the antenna cavity associated with the metal loss, dielectric loss and the switch-on resistance, as well as the leakage from the non-radiation edges. The latter is determined by how easily the antenna can couple the energy into the free space, on which regular bandwidth enhancement techniques such as using lower dielectric constants, wider patches and thicker substrates can be applied.

V. RADIATION EFFICIENCY ANALYSIS

It is well known that the efficiency bandwidth product in a conventional resonant antenna is approximately given by the inverse of the Q-factor

of the antenna [21]. One of essential merits of a DAM system is its better efficiency and bandwidth tradeoff relationship in transmission than that of conventional antennas, at the price of requiring special radiation waveforms and modulation formats. To obtain an efficiency bandwidth product greater than the usual limit, the switched patch antenna shown in Fig. 1 must radiate pulses for integer number of RF cycles. The position and the repetition rate of the pulses can be coded with the information to be transmitted [22]. Differing from conventional antennas, the radiation efficiency of a DAM system is defined as the ratio of the total radiated energy during the radiation period of each pulse $T_{r,pulse}$, to the total injected energy into the patch antenna during each Pulse Repetition Period (PRP). For pulse width or pulse position modulations, the data rate *C* is related to *PRP* as follows:

$$C = \frac{2}{PRP} \quad (bits/s). \tag{12}$$

The radiation efficiency can be evaluated by analyzing the charging and discharging behavior, based on the equivalent circuit models of the antenna during switch-on and off states. The complete derivation of the radiation efficiency of the DAM system based on the switched patch antenna is included in Appendix II. It concludes that the radiation efficiency for a given data rate *C* is as follows:

$$Eff_r = \frac{1}{\frac{1}{\xi} + (\frac{2}{CT_{r,pulse}} - 1)\frac{2Q_{off}}{Q_{on}}}, \tag{13}$$

ξ is the radiation-to-loss ratio of the radiation slot, defined as the total radiated energy over the total energy lost from the antenna in each RF cycle, including both the effective RF radiation and the dissipation caused by the switching action itself. A less than unit ξ indicates the dissipation of energy stored in the parasitic reactance surrounding the radiation slot due to the switching action, in the form of either spiky current flowing through the switch devices or spurious radiation into the free space. Q_{on} and Q_{off} are the intrinsic quality factors of the patch antenna resonator in the charging and discharging modes. (13) indicates that the maximum radiation efficiency of the DAM system is limited by the radiation-to-loss ratio ξ of the radiation edge. As the parasitic reactance of the radiation edge is often capacitive, one could maximize ξ by switching at the zero voltage moment if the carrier and the switching control can be synchronized with a phase locked loop. The zero voltage switching principle is similar to that in a high efficiency Class-E power amplifier [24]. In general, however, it is hard to achieve a high ξ for the patch antenna due to the complex nature of the parasitic effect at the radiation edge. Beside the limitation of ξ, either higher ratio of Q_{on} to Q_{off} or higher data rate *C* helps to achieve higher radiation efficiency, in contrast to a conventional antenna system where smaller bandwidth results in better efficiency. This is because the efficiency degradation in a DAM system is mainly caused by the resistive dissipation of switch devices. The loss is more significant when a longer charging period or PRP is used.

VI. SIMULATION RESULTS

To predict the performance of a DAM system, one needs to observe the interactions of waves and devices in the time-domain. For this purpose, a 3-D full wave simulator that incorporates switch models and resistive voltage sources is developed based on the extension of conventional 3-D dimensional FDTD algorithms [25]. A perfectly matched layer boundary condition is chosen to truncate the FDTD lattices. The time-domain near-to-far-field transformation approach described in [25], is implemented to obtain the time-domain radiation waveforms in the far field. The patch antenna is with dimensions of L=40.64 mm, W=80.77 mm, H=1.524 mm and the dielectric constant of the substrate ε_r = 2.33. 20 RF switch devices are mounted in parallel with uniform spacing 2.322 mm on the radiation edge of the antenna. Each RF switch device is chosen to have 0.2 Ω switch-on resistance and 2 MΩ switch-off resistance; therefore, the total switch-on/off resistance of the edge is 0.01 Ω and 20 kΩ, respectively. The resonant frequency during the switch-on period is 2.414 GHz. Figure 4 shows the FDTD simulation setup of the switched patch antenna. The antenna structure is discretized into 20×21×1 cells along X, Y and Z directions with the unit cell size of $2.032 \times 2.322 \times 1.524$ mm^3. The corresponding time step is $\Delta t = 3.6 ps$, which satisfies the Curant's stability criterion. 10-layer

Uniaxial Perfect Matched Layer (UPML) boundary conditions are used to truncate the FDTD lattices, which are placed at 16 cells away from the six sides of the antenna structure. The switching behavior is simulated by assuming the resistance of the switch varies from the switch-on value to the switch-off value according to an exponential function or vice versa. The transition time is 0.054 ns, which is about $1/8^{th}$ of the RF carrier cycle. The voltage source supplies a RF voltage of +/-10V and the source impedance of 160 Ω is used. The source is placed at the position shown in Fig. 5 to provide critical coupling at the feeding point to the antenna cavity. This means a perfect impedance match is obtained between the source and the load, e.g., the on-resistance of the switches in the steady state. Both RF switches and resistive voltage sources are formulated according to the modified FDTD updating equations for lumped element circuits in [25].

Both the original patch antenna and its cavity equivalent version in Fig. 1 are simulated. However, the strong leakage in the non-radiating slots in the original antenna limits the amount of energy storage during the switch-on period. Very little pulse compression gain (~2 dB maximum) can be achieved. To demonstrate a strong pulse compression effect, PMC boundary is placed at a half cell away from the two non-radiation edges to block the leakage from the non-radiating slots. Therefore, it is the patch antenna cavity in Fig. 1 (b) that is discussed in the following paragraphs. In practice, one may suppress the leakage by loading ferrite strips or placing multiple identical patches close to each other, side by side, to take advantage of the anti-phase property of the slots on both sides. To test the transient behavior of the antenna, it was first switched into the cavity mode to accumulate the input energy for about 253.6 ns. It is then switched to the radiating mode to radiate a single cycle of RF pulse (monopulse) that lasts for 0.418 ns. The PRP is 254 ns, which corresponds to a data rate of around 8 Mbits/s. Figure 5 shows the voltage waveform at the radiation edge of the patch for three pulses. It can be seen that the voltage waveform at the radiation edge appears to be smoothly regulated monocycle pulses. In order to calculate the pulse compression gain, one needs to compute the total radiated power carried by the pulse P_{rad}. This is done by integrating the radiated power at the far field in all directions. In addition to radiation, the energy lost per switching is included in the total energy flowing out of the radiation aperture during the pulse-on period with the average power of P_{av_a}. The radiation-to-loss ratio ξ can thus be evaluated as the ratio between these two. For this particular example, P_{rad}=0.738 W and P_{av_a}=4.6 W are obtained from FDTD simulations, which gives ξ=16%. In contrast, the maximum radiated power of the traditional microstrip patch antenna fed with the same single tone RF source is 0.078 W. Therefore, the maximum pulse compression gain is 9.75 dB. An alternative way in estimating the pulse compression gain is to first estimate the values of components in the equivalent transmission line model in Fig. 2, from the antenna dimensions then use (8) to evaluate the maximum pulse compression gain. For this particular example, the estimated component values are $Z_0 = 7.174\Omega$, $R_r = 615\Omega$ and $R_{on} = 0.01\Omega$. Therefore, the maximum pulse compression gain estimated by (8) is 9.15 dB, which agrees well with FDTD simulation results.

Figure 6 shows the time domain waveform of the radiated electric field at the broadside of the microstrip antenna. The distance of the observation point is $r=100\lambda_0$, where λ_0 is the free space wavelength of the RF carrier. It can be seen that the pulses appear accordingly in the far field when the switches are turned off and on periodically.

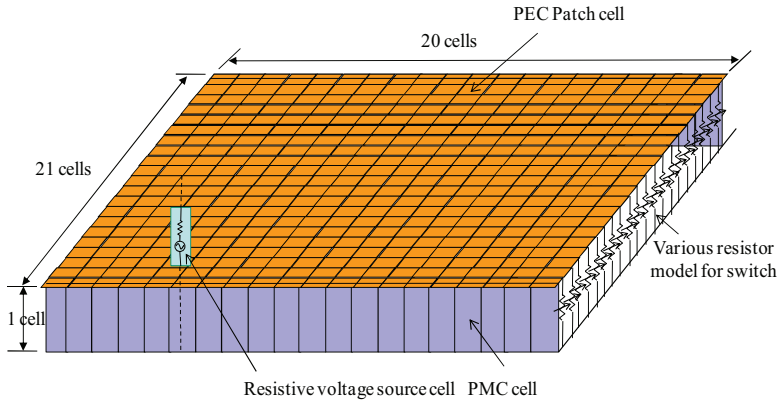

Fig. 4. FDTD simulation setup of the switched patch antenna.

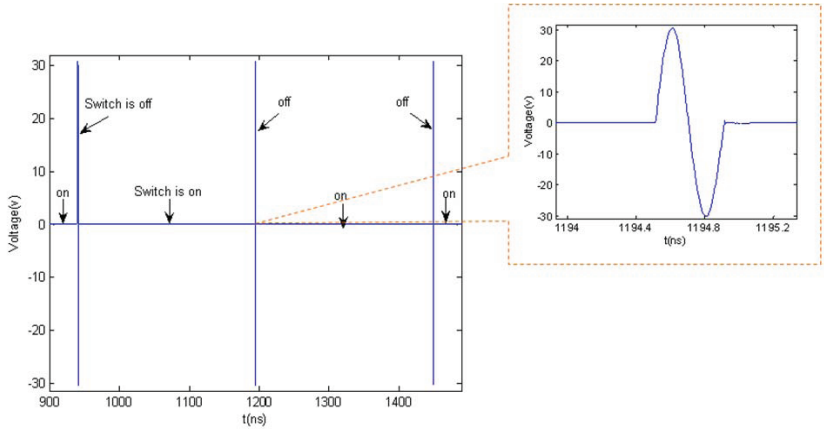

Fig. 5. Voltage waveform at the radiation edge of the switched patch antenna.

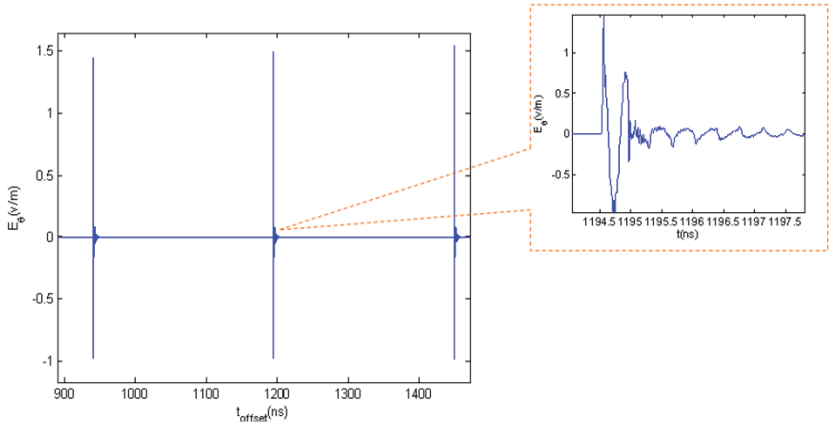

Fig. 6. Electric field waveform in far field at the broadside direction at the distance $r=100\lambda_0$.

As the waveform of a UWB signal radiated from an aperture antenna is dominated by the time derivative of the aperture field or magnetic current density in theory [26], the zoomed-in picture in Fig. 6 indeed shows a pulse waveform with discontinuities at the two edges, that is the time derivative of the monocylce aperture voltage. There is residue spurious radiation following the radiated pulse waveform even after the radiation is turned off. The spurious radiation is observed to be at much lower frequencies, which may be caused by releasing of the energy stored in the near field outside the antenna cavity after the switches short circuit the radiation slot. After

applying a time gate to remove the spurious noise, the frequency spectrum of the radiated electric field is shown in Fig. 7. The spectrum has a center frequency at around 2.77 GHz and a 3 dB bandwidth of 1.97 GHz, corresponding to a fractional bandwidth of 71%. It should be noted that the center frequency of 2.77 GHz in the radiation spectrum is shifted up from the original carrier frequency of 2.414 GHz. This is because the derivative effect in the radiated field adds an jw slope in the frequency response and emphasizes more in the higher frequency components. The center frequency returns to 2.414 GHz if the jw slope is de-embedded from Fig. 7. Given in Fig. 8 are the radiation patterns at the center frequency, the lower frequency and the upper frequency across the 3 dB bandwidth of the spectrum. Overall, the radiation patterns for the three examined frequencies are consistent in their shapes. The E-plane radiation patterns are almost identical for these three frequencies , though they are not perfectly symmetrical as only one radiation slot exists in the proposed microstrip patch antenna. This asymmetry causes the maximum radiation direction to shift away from the broadside to approximately the angle of $\theta = 20^{o}$. On the other hand, H-plane radiation patterns are perfectly symmetrical, while the patterns for higher frequencies show slightly narrower beamwidths due to the slightly higher antenna gains out of the same antenna aperture at higher frequencies.

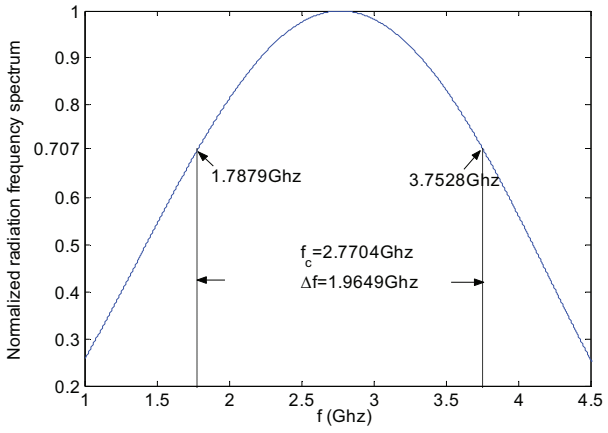

Fig. 7. Spectrum of the radiated monocycle pulse.

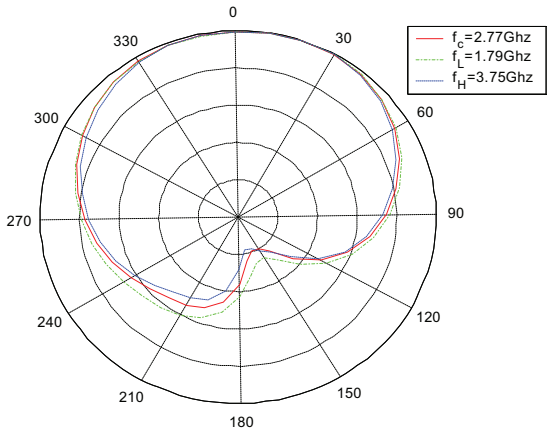

(a) E-plane

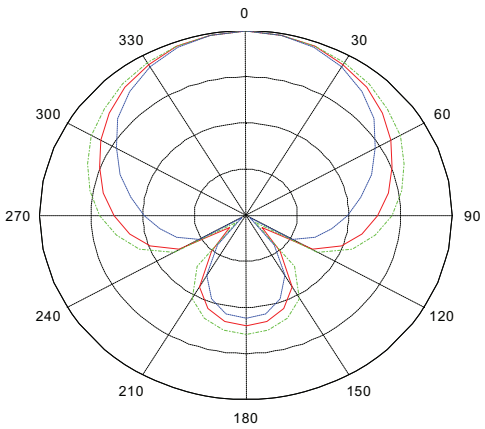

(b) H-plane

Fig. 8. Radiation patterns of 3 frequency components of the pulse in: (a) E-plane and (b) H-plane.

In DAM, one may operate the switched patch antenna toward higher radiation efficiency instead of higher pulse compression gain by using shorter charging time between the radiations. In order to examine the efficiency performance of the proposed scheme at different data rates, monopulses with different PRPs are used for communications that correspond to data rates up to 800 Mb/s. A comparison is carried out among three cases, as shown in Fig. 9. In the first case shown by the solid line, the radiation efficiency is strictly calculated from FDTD simulations by taking the ratio between the radiated energy and the injected energy. In the second case represented by the dotted line, the quality factors of the antenna resonator at both storage mode and

radiation mode and the radiation-to-loss ratio are obtained from the FDTD simulations. Those parameters are then substituted into (13) to predict the radiation efficiency. For the microstrip patch example shown in Fig. 1 (b), FDTD simulations show that $Q_{on} = 1256$, $Q_{off} = 167$ and $\xi = 16\%$. The FDTD prediction once again agrees well with the estimation given by (13). The third case is for a conventional microstrip patch antenna with the same physical dimensions as the DAM scheme, except the switches and the short-circuit is on the other radiating edge. A PMC boundary is also used to cover the non-radiating edges in this case. The efficiency is plotted in the dashed-dotted line. The radiation Q of the regular microstrip patch antenna obtained from FDTD simulations is around 200 at the resonant frequency of 2.4 GHz. For a conventional patch antenna, the radiation efficiency is almost 100% at the data rate of 12 Mb/s, as the modulation is within the antenna bandwidth. However, it is clear that the efficiency bandwidth product of this antenna is subject to the 1/Q limit, as the radiation efficiency drops quickly with the increase of the data rate. In contrast, the radiation efficiency of the proposed switched patch antenna scheme increases when the data rate increases and eventually saturates at the radiation-to-loss ratio of the radiation aperture $\xi = 16\%$. It is evident that the proposed switched patch antenna scheme can achieve 2-8 times higher radiation efficiency than the regular microstrip patch for data rates of 200 Mb/s and higher.

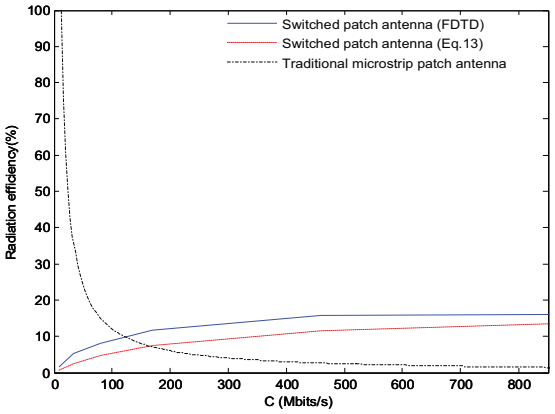

Fig. 9. Comparison of the radiation efficiency versus data rate between the DAM scheme and the conventional microstrip patch antenna.

VII. CONCLUSIONS

The theoretical performance of DAM technique is analyzed in this paper based on a switched patch antenna example. A thorough study on the time-varying behavior and nonlinear dynamics of this type of antennas has been carried out. The theoretical potential of the proposed antenna in terms of its radiation power and efficiency bandwidth relations have been derived by using both transmission line models and FDTD simulations. Both analyses and simulations demonstrated that the DAM scheme can obtain radiation efficiency bandwidth product over the conventional 1/Q limit, as long as pulses with integer number of RF cycles are transmitted as the information carrier and zero voltage switching is applied on the antenna.

Appendix I

For a resonator with a fixed intrinsic quality factor, one may prove that the electromagnetic energy stored in a resonator is maximized when the source impedance R_S is equal to the input impedance R_{in} of the resonator as follows. At the resonance, the intrinsic quality factor of the cavity according to the definition is given by:

$$Q = \omega_r \frac{2W_m}{P_{loss}} \quad \text{or} \quad Q = \omega_r \frac{2W_e}{P_{loss}}, \tag{A1}$$

where ω_r is the angular resonant frequency of the cavity, W_m, W_e are the average stored magnetic and electric energy which are equal to each other at resonance and P_{loss} is the dissipated power governed by:

$$P_{loss} = \frac{1}{2} V_S^2 \frac{R_{in}}{(R_S + R_{in})^2}. \tag{A2}$$

Substituting (A2) into (A1), the average stored magnetic/electric energy is given by:

$$W_m = W_e = \frac{Q}{4\omega_r} V_S^2 \frac{R_{in}}{(R_S + R_{in})^2}. \tag{A3}$$

To maximize the average stored magnetic/electric energy at resonance, the derivative of (A3) with respect to R_{in} must be zero, e.g.:

$$\frac{\partial W_m}{\partial R_{in}} = \frac{\partial W_e}{\partial R_{in}} = 0. \tag{A4}$$

By solving (A4), one yields:

$$R_{in} = R_S. \tag{A5}$$

The instantaneously radiated power from the antenna during the "pulse-on" period can be approximately obtained through the following transmission line analysis. To maximize the electromagnetic energy stored, the input impedance at the feeding position R_{in} should match to the source impedance R_S. Therefore, the feeding position L_1 needs to be adjusted to realize this matching. From the transmission line theory, the input admittance at the feeding point is given by:

$$G_{in} = Y_0 \frac{Y_{on} + jY_0 \tan(\beta L_1)}{Y_0 + jY_{on} \tan(\beta L_1)} + \frac{Y_0}{j \tan(\beta(L - L_1))}, \quad \text{(A6)}$$

where Y_{on} is the switch-on admittance and Y_0 is the transmission line characteristic admittance of the patch. Substituting the resonance condition $\beta L = \pi$ and the condition $Y_{on} >> Y_0$ into (A6), G_{in} is reduced approximately to:

$$G_{in} \approx \frac{1}{\sin^2(\beta L_1)} \frac{Y_0^2}{Y_{on}}. \quad \text{(A7)}$$

Substituting the matching condition $R_{in} = R_s$ yields:

$$\sin(\beta L_1) = \frac{\sqrt{R_s R_{on}}}{Z_0}, \quad \text{(A8)}$$

which determines the feeding position. When the switches are on, the voltage distribution along the equivalent transmission line of the patch follows a sinusoid function, which means that the voltage reaches maximum V_m in the middle of the line and is approximately zero at both ends. Therefore, the input voltage at the feeding point V_i is given by:

$$V_i = V_m \sin(\beta L_1). \quad \text{(A9)}$$

As any standing wave in resonators can be decomposed into two traveling waves that propagate toward opposite directions, the maximum voltage of the standing wave along the line should be equal to the summation of the amplitudes of both forward and backward propagating waves. This gives the amplitude of the traveling waves:

$$V_m^+ = V_m^- = \frac{1}{2} V_m = \frac{1}{2} \frac{V_i}{\sin(\beta L_1)}. \quad \text{(A10)}$$

The amplitude of incident wave V_{edge}^+ at the edge of the switches is equal to V_m^+ from the definition of traveling waves:

$$V_{edge}^+ = V_m^+ = \frac{1}{2} \frac{V_i}{\sin(\beta L_1)}. \quad \text{(A11)}$$

The reflected wave should be approximately equal to the incident wave in amplitude but with the opposite sign, so that the total edge voltage is approximately zero because of the low switch resistance condition at the edge. After the cavity is fully charged, the switches are turned off. The boundary condition at the switch edge suddenly changes from low impedance to high impedance. An enhanced aperture field should appear on this edge right after the switching moment. The voltage at the edge is thus given by:

$$V_{edge} = V_{edge}^+ + V_{edge}^- = V_{edge}^+ (1 + \Gamma), \quad \text{(A12)}$$

where Γ is the reflection coefficient at the edge, which is determined by the aperture radiation impedance. The reflection coefficient is given by:

$$\Gamma = \frac{\frac{1}{G_r + jB_r} - Z_0}{\frac{1}{G_r + jB_r} + Z_0}, \quad \text{(A13)}$$

thus,

$$V_{edge} = V_{edge}^+ \left[\frac{2}{1 + Z_0 (G_r + jB_r)} \right]. \quad \text{(A14)}$$

The radiation resistance $R_r = 1/G_r$ is usually much greater than the characteristic impedance Z_0 for practical microstrip antennas. Therefore, the instantaneous voltage at the edge is somehow "amplified." The instantaneous power radiated is given by:

$$P_{rad} = \frac{1}{2} |V_{edge}|^2 G_r. \quad \text{(A15)}$$

Substituting (A10) and (A14) into (A15) yields:

$$P_{rad} = \frac{1}{2} \frac{V_i^2}{R_s} \frac{Z_0^2 G_r}{R_{on}} \frac{1}{(1 + Z_0 G_r)^2 + (Z_0 B_r)^2}. \quad \text{(A16)}$$

As for an ideal regular patch antenna excited with a single-tone carrier supply in the same amplitude, the maximum radiated power is equal to the injected power $P_{rad} = \frac{1}{2} \frac{V_i^2}{R_s}$. Under the assumption of $G_r Z_0 << 1$ and $B_r << Y_0$, the maximum pulse compression gain is thus derived to be:

$$G_{pulse,\max} = \frac{Z_0^2}{R_{on} R_r}. \quad \text{(A17)}$$

Appendix II

The equivalent circuits of the antenna in both charging and discharging states are depicted in Fig. A1.

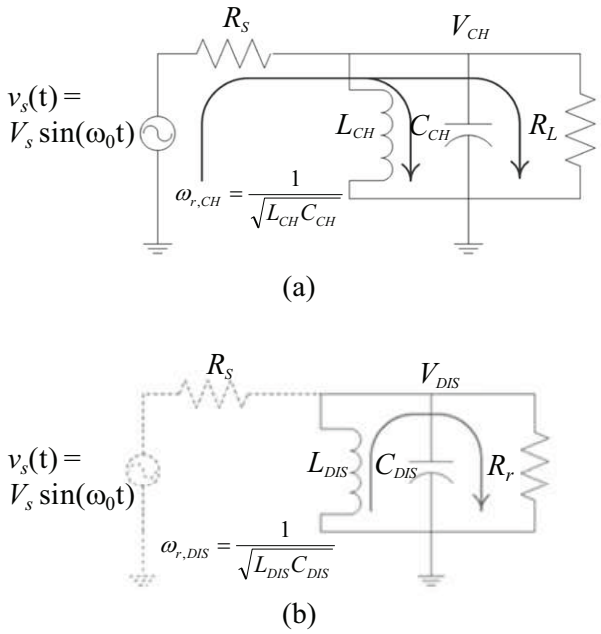

Fig. A1. (a) Charging and (b) discharging mode equivalent circuit models of the switched patch antenna.

Figure A1 (a) represents the charging behavior of the antenna, where R_S is the source resistance and R_L is the transformed load resistance from the switch-on resistance of the RF switches; L_{CH} and C_{CH} are the equivalent inductance and capacitance of the switched patch antenna resonator during the charging mode. The patch antenna resonator is charged according to the time constant $\tau_{CH} = (R_S // R_L)C_{CH}$. Once the switches are turned off, the source is removed and the antenna starts to discharge due to the radiation, as represented by Fig. A1 (b). Assuming that the switch-off resistance is much greater than the radiation resistance of the antenna, the discharging time constant is governed by $\tau_{DIS} = R_r C_{DIS}$, where R_r is the radiation resistance of the radiation slot and C_{DIS} is the equivalent capacitance of the switched patch antenna resonator in the discharging mode. If the switched patch antenna resonator is excited at the resonance during the charging mode, with the resonant frequency $\omega_0 = \omega_{r,CH}$, the voltage change during the charging time Δt_{CH} and the discharging time Δt_{DIS} can be written as the follows [20]:

$$\Delta V_{CH} = (V_{DIS}(t_1) - V_{CH,Steady})(-\Delta t_{CH} / 2\tau_{CH}), \quad \text{(A18 (a))}$$

$$\Delta V_{DIS} = (V_{CH}(t_0) - V_{DIS,Steady})(-\Delta t_{DIS} / 2\tau_{DIS}), \quad \text{(A18 (b))}$$

where $V_{CH,Steady}$ and $V_{DIS,Steady}$ stand for the steady state voltages of the antenna resonator after the infinite amount of charging and discharging time, in which $V_{CH,Steady} = V_S /(R_S / R_L + 1)$ and $V_{DIS,Steady} = 0$. $V_{DIS}(t_1)$ is the initial condition of the resonator at the switching moment when discharging ends and charging begins. $V_{CH}(t_0)$ is the initial condition of the resonator in the discharging mode, which is the voltage when charging ends and discharging starts. With the switching process repeating for a certain period of time, the voltage changes during the charging and discharging modes and must settle to be equal, due to the equilibrium,

$$\Delta V_{CH} = \Delta V_{DIS}. \quad \text{(A19)}$$

Under the assumption that the switching speed is much faster than the resonator bandwidth, the initial voltages of $V_{DIS}(t_1)$ and $V_{CH}(t_0)$ can be approximated by the settling voltage V_X:

$$V_X \approx V_{CH}(t_0) \approx V_{DIS}(t_1). \quad \text{(A-20)}$$

Substituting Eqs. (A18) and (A20) into Eq. (A19):

$$(V_{CH,Steady} - V_X)\frac{\Delta t_{CH}}{\tau_{CH}} = V_X \frac{\Delta t_{DIS}}{\tau_{DIS}}. \quad \text{(A21)}$$

Thus, the settling voltage ratio $\eta_{Settling}$, defined as the ratio between the settling voltage and the steady voltage $V_{CH,Steady}$ is given by:

$$\eta_{Settling} = \frac{V_X}{V_{CH,Steady}} = \frac{1}{1 + \frac{\Delta t_{DIS}}{\Delta t_{CH}} \frac{\tau_{CH}}{\tau_{DIS}}}. \quad \text{(A22)}$$

The charging and discharging time constants can also be expressed in terms of the intrinsic quality factors of the patch antenna resonator, respectively, in the charging and discharging modes Q_{on} and Q_{off}. The charging time constant is:

$$\tau_{CH} = Q_{on} /(R_L / R_S + 1)\omega_{r,CH}), \quad \text{(A23)}$$

where $\omega_{r,DIS} = \omega_{r,CH} / 2$ because of the change of the resonant frequency from the l/2 mode to the l/4 mode. The discharging time constant is then governed by:

$$\tau_{DIS} = Q_{off}\xi/(\omega_{r,DIS}), \quad \text{(A24)}$$

as the radiation-to-loss ratio ξ is defined as the ratio of the total radiated energy from the per RF cycle to the total energy loss per RF cycle, including both the radiation and the loss, due to the switching action itself. Substituting the relations $\Delta t_{DIS} = T_{r,pulse}$ and $\Delta t_{CH} = PRP - T_{r,pulse}$; Eqs. (A23) and (A24) into (A22) yields:

$$\eta_{Settling} = \frac{1}{1+\frac{1}{PRP/T_{r,pulse}-1}\frac{Q_{on}/(R_L/R_S+1)}{2Q_{off}\xi}}, \quad \text{(A25)}$$

or,

$$\eta_{Settling} = \frac{1}{1+\frac{1}{2/(CT_{r,pulse})-1}\frac{Q_{on}/(R_L/R_S+1)}{2Q_{off}\xi}}, \quad \text{(A26)}$$

where C is the data rate of the system which is related to PRP by:

$$C = \frac{2}{PRP} \quad (bits/s). \quad \text{(A27)}$$

(A26) shows that a higher settling operating point results from a lower data rate or smaller duty cycle of the radiated pulses, for a given patch antenna design and matching condition. On the other hand, the voltage envelop across the resonant LC tank resulting from the initial charging process is:

$$V_{CH}(t) = V_S/(R_S/R_L+1)(1-e^{-t/2\tau_{CH}}). \quad \text{(A28)}$$

The voltage finally settling across the LC tank in the charging mode is thus:

$$V_{CH}(\eta_{Settling}) = V_S/(R_S/R_L+1)\eta_{Settling}. \quad \text{(A29)}$$

From KCL circuit theory, the total settling current flowing into the LC tank in charging mode is given by:

$$I_{CH}(\eta_{Settling}) = V_S(1-\frac{\eta_{Settling}}{R_S/R_L+1})/R_S. \quad \text{(A30)}$$

The time-average input power into the LC tank in the charging mode is:

$$P_{CH}(\eta_{Settling}) = \frac{V_S^2}{2}\frac{\eta_{Settling}}{R_S/R_L+1}(1-\frac{\eta_{Settling}}{R_S/R_L+1})/R_S. \quad \text{(A31)}$$

The time-average dissipated power on the equivalent resistance R_L is:

$$P_d(\eta_{Settling}) = \frac{V_S^2}{2}(\frac{\eta_{Settling}}{R_S/R_L+1})^2/R_L. \quad \text{(A32)}$$

When the resonator is settling at the highest point ($\eta_{Settling}=1$),

$$P_{CH}(\eta_{Settling}=1) = P_d(\eta_{Settling}=1) = \frac{V_S^2}{2}(\frac{1}{R_S/R_L+1})^2/R_L, \quad \text{(A33)}$$

the input power is completely dissipated on the switches, while the stored energy in the LC tank reaches its maximum. This is the condition for the maximum pulse compression gain. However, to achieve higher radiation efficiency requires $\eta_{Settling}<1$, whereas the pulse compression gain drops accordingly,

$$G_{pulse}(\eta_{Settling}) = \eta_{Settling}^2 G_{pulse,\max}. \quad \text{(A34)}$$

Based on the definition of the pulse compression gain, the average radiated power from the radiation pulse is given by:

$$P_{r,pulse}(\eta_{Settling}) = G_{pulse}(\eta_{Settling})P_{r,patch}. \quad \text{(A35)}$$

A conventional resonant patch antenna has the same equivalent circuit model as that in Fig. A1 (a), where R_L is the transformation of the radiation impedance of the antenna if other types of loss are ignored. With the same resistive voltage source as the switched patch antenna, the maximum radiated power of the traditional patch antenna $P_{r,patch}$ will be equal to the maximum dissipated power on the switches of the antenna resonator during the switch-on period, e.g.:

$$P_{r,patch} = P_d(\eta_{Settling}=1). \quad \text{(A36)}$$

Substituting Eqs. (A34) and (A36) into (A35), the time-average radiated power for the pulse is obtained,

$$P_{r,pulse}(\eta_{Settling}) = P_d(\eta_{Settling}=1)G_{pulse,\max}\eta_{Settling}^2. \quad \text{(A37)}$$

Thus, the total radiated energy is:

$$E_{r,pulse}(\eta_{Settling}) = P_{r,pulse}(\eta_{Settling})\Delta t_{DIS}. \quad \text{(A38)}$$

It is assumed that the radiation takes a small portion of the total stored energy away from the antenna resonator, due to the short radiation period. Due to energy conservation, the total input energy into the antenna resonator during the recharging period is to recuperate the amount of stored energy that was lost in the previous discharging state, which is denoted by E_{rc} and to compensate the dissipated energy on the switches E_d during the recharging period at the same time. By recalling the definition of the radiation efficiency of the switched patch antenna, we have:

$$Eff_r(\eta_{Settling}) = \frac{E_{r,pulse}(\eta_{Settling})}{E_{rc}(\eta_{Settling})+E_d(\eta_{Settling})}. \quad \text{(A39)}$$

The recuperated energy E_{rc} is equal to the total stored energy loss during the radiation period $T_{r,pulse}$, caused by both the radiation from the radiation edge and the switching action itself. Therefore,

$$E_{rc}(\eta_{Settling}) = E_{r,pulse}(\eta_{Settling})/\xi . \quad \text{(A40)}$$

The dissipated energy on the switches during the recharging period is given by:

$$E_d(\eta_{Settling}) = P_d(\eta_{Settling}=1)\eta_{Settling}^2 \Delta t_{CH} , \quad \text{(A41)}$$

where,

$$\Delta t_{CH} = \frac{E_{rc}(\eta_{settling})}{P_{CH}(\eta_{settling}) - P_d(\eta_{settling})} . \quad \text{(A42)}$$

After substituting Eqs. (A38), (A40), (A26) and (A39) into (13) and some additional mathematical manipulations, the radiation efficiency of the pulse transmission scheme based on the switched resonant patch antenna in Fig. 1 is finally obtained,

$$Eff_r = \frac{\xi}{1+(\frac{2}{CT_{r,pulse}}-1)\frac{2Q_{off}\xi}{Q_{on}}} . \quad \text{(A43)}$$

REFERENCES

[1] H. G. Schantz, "Introduction to ultra-wideband antenna," *IEEE UWBST 2003 Conference Proceedings*, pp. 1-9, November 2003.

[2] H. G. Schantz, "A brief history of ultra-wideband antennas," *IEEE UWBST 2003 Conference Proceedings*, pp. 209-213, November 2003.

[3] K. Y. Yazdandoost and R. Kohno, "Ultra-wideband antenna," *IEEE Communications Magazine*, vol. 42, pp. 29-32, June 2004.

[4] J. T. Merenda, "Synthesizer radiating systems and methods," *U.S. Patent No. 5,402,133*, March 28, 1995.

[5] V. F. Fusco and Q. Chen, "Direct-signal modulation using a silicon microstrip patch antenna," *IEEE Trans. on Antenna and Propagation*, vol. 47, pp. 1025-1028, June 1999.

[6] W. Yao and Y. Wang, "Radiating beyond the bandwidth using direct antenna modulation," *Antennas and Propagation Society International Symposium, IEEE*, vol. 1, pp. 20-25, June 2004.

[7] W. Yao and Y. Wang, "Direct antenna modulation-a promise for ultra-wideband (UWB) transmitting," *Microwave Symposium Digest, IEEE MTT-S International*, vol. 2, pp. 1273-1276, June 2004.

[8] S. D. Keller, W. D. Palmer, and W. T. Joines, "Direct antenna modulation: analysis, design, and experiment," *IEEE Antennas and Propagation Society International Symposium 2006*, pp. 909-912, July 9-14, 2006.

[9] S. D. Keller, W. D. Palmer, and W. T. Joines, "Digitally driven antenna for HF transmission," *IEEE Trans.* on *Microwave Theory and Techniques*, vol. 58, no. 9, pp. 2362-2367, September 2010.

[10] H. G. Schantzchantz, "Nanoantennas: a concept for efficient electrically small UWB devices," *2005 IEEE International Conference on Ultra-Wideband*, pp. 264-268, September 5-8, 2005.

[11] J. Wang, "Characteristics of a new class of diode-switched integrated antenna phase shifter," *IEEE Trans. Antennas and Propagation*, vol. 31, pp. 156-159, January 1983.

[12] F. Yang and Y. Rahmat-Samii, "A reconfigurable patch antenna using switchable slots for circular polarization diversity," *IEEE Microwave and Wireless Components Letters*, vol. 12, no. 3, pp. 96-98, March 2002.

[13] G. H. Huff, J. Feng, S. Zhang, and J. T. Bernhard, "A novel radiation pattern and frequency reconfigurable single turn square spiral microstrip antenna," *IEEE Microwave and Wireless Components Letters*, vol. 13, pp. 57-59, February 2003.

[14] A. E. Fathy, A. Rosen, H. S. Owen, F. McGinty, D. J. McGee, G. C. Taylor, R. Amantea, P. K. Swain, S. M. Perlow, and M. ElSherbiny, "Silicon-based reconfigurable antennas-concepts, analysis, implementation, and feasibility," *IEEE Trans. Microwave Theory and Techniques*, vol. 51, pp. 1650-1661, June 2003.

[15] J. T. Aberle, S. H. Oh, D. T. Auckland, and S. D. Rogers, "Reconfigurable antennas for wireless devices," *IEEE Trans. Antennas and Propagation Magazine*, vol. 45, pp. 148-154, December 2003.

[16] V. P. Prokhorenko, V. E. Ivashchuk, and S. V. Korsun, "Electromagnetic impulse radiator," *Ultrawideband and Ultrashort Impulse Signals*, Sevastopol, Ukraine, pp. 243-245, September 19-22, 2004.

[17] V. P. Prokhorenko, V. E. Ivashchuk, and S. V. Korsun, "On radiation efficiency and radiating capability of impulse antennas," *Ultrawideband and Ultrashort Impulse Signals*, Sevastopol, Ukraine, pp. 251-253, September 19-22, 2004.

[18] V. P. Prokhorenko, V. E. Ivashchuk, and S. V. Korsun, "Improvement of electromagnetic pulse radiation efficiency," *Subsurface Sensing Technologies and Applications*, vol. 6, pp. 107-123, April 2005.

[19] X. Xu, H. C. Jing, and Y. E. Wang, "High speed pulse radiation from switched electrically small antenna," 2006 IEEE *AP-S International Symposium and USNC/URSI National Radio*

Science Meeting, Albuquerque, New Mexico, July 2006.

[20] R. Harrington, "Effects of antenna size on gain, bandwidth, and efficiency," *Journal of Research of National Bureau of Standards*, v 64-D, pp. 1-12, 1960.

[21] S. Kim and Y. E. Wang, "Theory of switched RF resonators," *IEEE Trans. Circuits and Systems*, vol. 53, pp. 2521-2527, December 2006.

[22] H. Liu, "Error performance of a pulse amplitude and position modulated ultra-wideband system over lognormal fading channels," *IEEE Comm. Letters*, vol. 7, no. 11, pp. 531-533, November 2003.

[23] C. A. Balanis, "Antenna theory: analysis and design," Third Edition, *John Wiley & Sons, Inc*, 2005.

[24] F. Raab, "Idealized operation of the class e tuned power amplifier," Circuits and Systems, *IEEE Trans. Circuits and Systems*, vol. 24, no. 12, pp. 725-735, December 1977.

[25] A. Taflove and S. C. Hagness, "Computational electrodynamics: the finite-difference time-domain method," Second Edition, *Artech House*, 2000.

[26] C. E. Baum, "Radiation of impulse-like transient fields," *Sensor and Simulation Notes 321 USAF Phillips Lab*, Albuquerque, NM, November 1989.